Chinese Chemical Letters 33 (2022) 5013–5022

Contents lists available at ScienceDirect

Chinese Chemical Letters

journal homepage: www.elsevier.com/locate/cclet

Recent advances in the application of metal organic frameworks using in advanced oxidation progresses for pollutants degradation

Heshan Zheng[a], Yunying Hou[a], Shuo Li[a,b,c,*], Jun Ma[b,c], Jun Nan[b,c], Tong Li[d,*]

[a] College of Chemistry and Chemical Engineering, Qiqihar University, Qiqihar 161006, China
[b] Urban Water Resources Development and Northern National Engineering Research Center, Harbin 150090, China
[c] School of Environment, Harbin Institute of Technology, Harbin 150090, China
[d] School of Energy and Environmental Engineering, University of Science and Technology Beijing, Beijing 100083, China

ARTICLE INFO

Article history:
Received 31 October 2021
Revised 11 December 2021
Accepted 17 January 2022
Available online 23 January 2022

Keywords:
Advanced oxidation progresses
Metal-organic frameworks
Contaminants degradation
Synthesis methods
Catalysis mechanism

ABSTRACT

Metal-organic frameworks (MOFs) materials with highly ordered and porous crystalline structure, have excellent performance in advanced oxidation progresses (AOPs) for organic contaminants degradation in water treatment. This review intends to summarize the timely references and insights for the recent advances in MOFs that are used in AOPs. Starting with the preparation methodologies, including conventional hydrothermal method, electrochemical method, sol-gel method, and emerging microwave and ultrasound assisted synthesis methods. Application and mechanism for MOFs using in various AOPs of Fenton-like, photocatalysis, catalytic ozonation, persulfate catalysis and other emerging oxidation methods are emphatically discussed. We hope this review can comprehensively summarize the research and application progress of MOFs in AOPs, deepen the understanding of the catalytic mechanisms.

1. Introduction

Due to the continuous increase in industrial production and living demands, some emerging contaminants of pharmaceuticals and personal care products (PPCPs), endocrine disrupting compounds (EDCs), polycyclic aromatic hydrocarbons (PAHs) and polychlorinated biphenyl (PCBs), are continuously accumulated in environment. Those emerging pollution caused potential threats and direct harm to the ecological environment and human health [1–4], such as affecting human reproduction, metabolism and neurodevelopment, even causing cancer, deformity, mutation and death [5,6]. Hence, academics have begun to develop new methods to control and reduce the contaminants in aqueous environment. The treatment methods include anode degradation, biodegradation, inorganic heterogeneous catalysis and activated carbon adsorption, *etc.* [7–9]. However, these technologies have diverse limitations of pollutants transfer, incomplete degradation and high energy requirements. For example, anode degradation needs high operating costs and challenging problems with fouling. Adsorption techniques have problems with the recovery and disposal of irreversible adsorbents.

Advanced oxidation progresses (AOPs) could degrade organic pollutants by generating hydroxyl radicals (•OH), superoxide radicals ($O_2^{\bullet-}$), and sulfate radicals ($SO_4^{\bullet-}$) that with strong oxidizing. A variety of AOPs, such as electrochemical oxidation, Fenton, ozone oxidation and photocatalysis, have been widely developed and applied [10,11]. The central issue of AOPs is developing new catalysts that act as absolute domination for activity oxide species and their catalytic performances.

In 1995, Omar M. Yaghi [12] synthesized a ligand compound with a two-dimensional structure composed of rigid organic ligand 1,3,5-benzenetricarboxylate (BTC) and transition metal Co, and named as metal-organic framework (MOF). However, MOFs did not attract much attention due to the materials were not stable at that time. By 1999, the Yaghi's research team [13] reported on a three-dimensional metal organic framework material MOF-5 with a simple cubic structure made of rigid organic ligand terephthalic acid and transition metal Zn. And the skeleton of MOF-5 remained intact after removing the guest molecules in the pores. This phenomenon attracted the attention to scholars and made MOFs develop rapidly. As shown in Fig. 1, the number of papers about MOFs is increasing during the past decade. The tunability of MOFs originated from the fact that various metal sites and organic ligands can constantly change and combine with each other to form another structure [14]. Tens of thousands of MOFs have been prepared and applied for catalytic synthesis [15,16], drug delivery [17], separation and storage of gas [18,19], electrode material [20] and fuel cells [21], *etc.*

* Corresponding authors.
E-mail addresses: shuo_105@163.com (S. Li), litong619@ustb.edu.cn (T. Li).

https://doi.org/10.1016/j.cclet.2022.01.048
1001-8417/

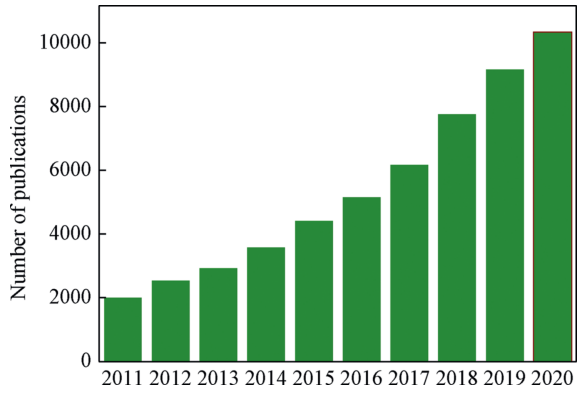

Fig. 1. The number of publications in the area of MOFs from 2011 to 2020 (research Web of Science on Sep. 10, 2021, MOFs research volume growth trend).

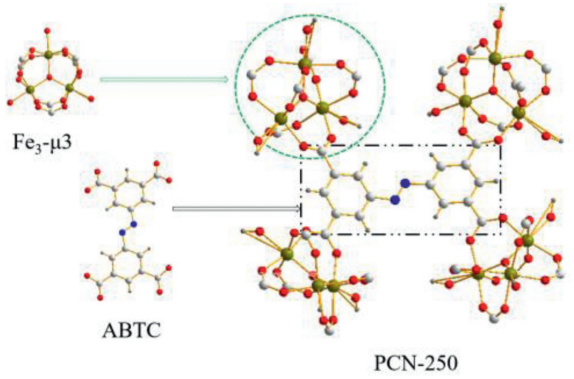

Fig. 2. The PCN-250(Fe_3) building unit composed of Fe_3-μ3-oxo clusters and 3,3′,5,5′-azobenzenetetracarboxylate (ABTC). Reproduced with permission [35]. Copyright 2020, American Chemical Society.

Recently, MOFs are used to deal with various environmental issues in adsorption of heavy irons, degradation of organic pollutants in wastewater [22–24], or separation and adsorption of carbon dioxide and sulfur dioxide [25–27]. As compared to heterogeneous catalysts, MOFs have adjustable structure and designable catalytic center, which is easy to recycle than homogeneous catalysts [28,29]. Therefore, AOPs, which need new catalysts to improve the effect of wastewater treatment, combined with a new functional environmental remediation materials MOFs, have been used by scholars to remove organic pollutants from water [24]. You *et al.* [30] used NiZn@doped graphite activated peroxymonosulfate to degrade bisphenol A in water. Hu *et al.* [31] carbonized Co/NH_2−MIL-88B(Fe) at high temperature in N_2 to obtain MOF derived nitrogen doped porous carbon rod (Fe_2Co_1/NPC), which removed 91% of 20 mg/L tetracycline within 60 min in electro-Fenton progress.

This paper summarizes the latest advances in MOFs as catalyst in AOPs and their catalytic degradation mechanisms for various pollutants. This carefully prepared review is hoped to promote the development of this kind of materials and their practical applications for water treatment.

2. Materials composition and function of MOFs

Both metal center and organic ligand are two important components of MOF materials. The catalytic process of MOFs in AOPs is originated from the adsorption of pollutants by the pores of the material and then oxidation by active group or free radicals generated from active sites. Therefore, both the metal center and organic structure will affect the catalytic performance of MOFs.

2.1. Catalytic core of metal center

Generally, metals serve as central role in MOFs can be divided into two categories of single and multiple metal centers. The change of the metal center will affect its surface morphology, and further affect the catalytic activity of the catalyst [32]. For instance, Ahmad *et al.* [33] synthesized CUCs-MIL-88B-Fe with a coordinated unsaturated metal center (CUC) to degrade phenol and sulfamethoxazole (SMX) in photo-Fenton process. From the scanning electronic microscopy (SEM) results, MIL-88B-Fe showed length of around 1 mm with long smooth surfaces. Surface of CUCs-MIL-88B-Fe was a little bit rough and course with evenly distributed pores. The former transform infrared spectroscopy and Barrett-Joyner-Halenda results showed that water molecules and hydroxyl groups were eliminated, and formated mix-valence Fe^{II}/Fe^{III} which led CUCs-MIL-88B-Fe to presented micro and mesopores. These results manifested that the introduction to coordinated unsaturated iron centers could create $^{\bullet}OH$ by mesopores in CUCs-MIL-88B-Fe along with inherent micropores. Taha *et al.* [34] respectively synthesized NH_2−MIL-101(Fe) and NH_2−MIL-101(Al) with Fe and Al as metal centers, which were applied for Fenton-like oxidation system. The surface area of NH_2−MIL-101(Fe) was 2572.5 m^2/g, 1.24 times of NH_2−MIL-101(Al). Within 5 min, the degradation rate of Rhodamin B (RhB) could be exceeded to 99% by NH_2−MIL-101(Fe), while the degradation rate of RhB by Al-based NH_2−MIL-101 was only 76.51% [34]. This study indicated that catalytic activity in NH_2−MIL-101 could be greatly affected by catalytic center in same MOF.

Moreover, the degradation capacity for organic contaminants of MOFs could be enhanced by using other transition metals to instead. Kirchon *et al.* [35] synthesized PCN-250(Fe_2Mn) with Mn instead of Fe (Fig. 2). Compare with the 1460 m^2/g BET area and 711.2 eV binding energy of PCN-250(Fe_3), PCN-250(Fe_2Mn) had 1472 m^2/g of surface area and lower binding energy (710.9 eV) displacement, which indicated that the isomorphic substitution of Mn for Fe could bring faster electron transfer rate and higher oxidation capacity for methylene blue (MB) degradation in photo-Fenton.

The identity of metal oxidation state and rations of MOFs are also the key issue for their high degradation efficiency. Tang *et al.* [36] reported $Fe_{0.75}Cu_{0.25}$(BDC) could degrade SMX completely within 120 min in Fenton-like system. Different from octahedral Fe(BDC) and cubic layered Cu(BDC), $Fe_{0.75}Cu_{0.25}$(BDC) was formed in an irregular flake-like structure. The incorporation of copper enhanced pore size and Fe(II) of $Fe_{0.75}Cu_{0.25}$(BDC). Moreover, [Fe,Cu]-BDC was utilized as precursor to obtain a three-dimensional flower-like FeCu@C by pyrolysis [37]. FeCu@C had a higher particle size (100–300 nm width and 1–2.5 μm length), less agglomerated structure, more dispersed active center and better permeability than Fe/C (its particle size was 100–200 nm). Under oxidation progress of H_2O_2 catalyzed by FeCu@C, sulfamethazine (SMT) could be completely removed in 90 min. Xie *et al.* [38] synthesized Ag_3PO_4/MIL-53(Fe) by tightly anchoring Ag_3PO_4 nanoparticles on the surface of MIL-53(Fe). Ag_3PO_4/MIL-53(Fe) exhibited more active sites and larger surface area of 15.525 m^2/g, 1.82 times than pure MIL-53(Fe). In addition to directly synthesizing MOFs with bimetallic centers, catalytic efficiency of the MOF can also be enhanced by introducing additional active sites. Liu *et al.* [39] introduced Co into Zn-MOF and prepared a bimetallic site catalyst Zn/Co-MOF. Du *et al.* [40] doped Zn^{2+} and Cu^{2+} ions into Mn^{2+}-based MOF (STU-2) to obtain a robust hetero metallic MOF, of that material had high heterogeneous catalytic performance for the cyano-silylation of aromatic aldehydes and high stability.

Therefore, changes in metal sites, coordination unsaturated metal sites or metal complexes will affect the shape and size of

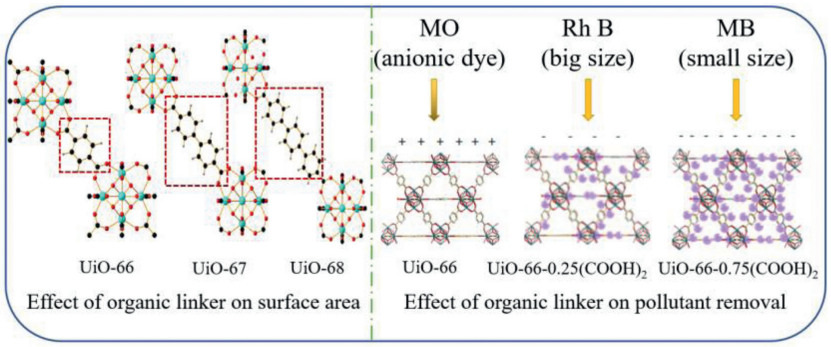

Fig. 3. Effect of organic linker on surface area and pollutant removal. Reproduced with permission [42,46]. Copyright 2008, American Chemical Society; Copyright 2018, Elsevier.

the pores, even change the structure of the material and thereby affecting its catalytic performance.

2.2. Organic ligands of MOFs

MOFs catalytically degrade pollutants in two steps of pollutants adsorption and then reacting with the catalytic sites or active groups of MOFs. Therefore, both pore diameter and pore volume of organic linkers play significant roles in the progress of contaminants removal. As an essential part of organic linker is mainly used as a frame structure to connect various metal centers to form channels with various pore diameters, which can promote highly dispersed reactant molecules to enter the inner surface to independently react with each metal site.

Generally, the chain length of the organic ligand is long to obtain a larger size and specific surface area. Wang *et al.* [41] synthesized NH_2−MIL-88B(Fe) with 2-aminoterephthalic acid, and then synthesized various MOFs (the corresponding MOFs were named Bac-MIL88(Fe), Py-MIL88(Fe) and Pca-MIL88(Fe), respectively) by doping with different organic ligands (benzoic acid, pyrrole and pyrrole-2-carboxylic acid) used for photo-Fenton to degrade acetamide. The adsorption efficiency of these materials was consistent with the surface area and pore volume increased in the order of MIL88(Fe) < Bac-MIL88(Fe) < PyMIL88(Fe) < Pca-MIL88(Fe).

Similarly, Fig. 3 clearly showed that the structure of Zr-MOF (UiO-66, UiO-67 and UiO-68) changed with the length of the linkers [42]. The surface area of UiO-66 with only one benzene ring as the organic linker was 1187 m^2/g. When linkers were expanded to two and three benzene ring dicarboxylic acids, the surface area of UiO-67 and UiO-68 could increase to 3000 and 4170 m^2/g, respectively [42]. With the increase of the number of benzene rings, their specific surface areas increased by 1.5 times and 2.5 times, respectively. Meantime, according to the research of Duren *et al.* [43], the van der Waals surface area per volume of chain structure is about twice that of nonchain structure. Therefore, MOFs obtained by changing the organic ligands with same metal site can adjust the specific surface area, diameter and pore size. However, a major disadvantage of MOFs with abnormally high surface area is weak stability. When the organic frame of the material is too long, it is easy to cause the collapse of the cavity. Therefore, the synthesis of an economical and efficient MOF is the key research direction of MOFs.

When the pore diameter of MOFs is not large enough, the reaction rate will be limited by the diffusion of reagents and products, due to channels are too small to capture contaminants. Yu *et al.* [44] used terephthalic acid and 1,3,5-benzenetricarboxylic acid to synthesize MIL-53(Fe) and MIL-100(Fe) for catalytic ozonation. The pore size of MIL-100(Fe) was 4.25 nm, while MIL-53(Fe) was only 2.96 nm. The adsorption experiment showed that MIL-100(Fe) removed 74.3% of RhB within 10 min, 1.13 times that of MIL-53(Fe). The high catalytic performance comes from its abundant active sites and large specific surface area. Taha *et al.* [34] synthesized MIL-101(Fe) and NH_2−MIL-101(Fe) with BET surface areas of 2122.6 m^2/g and 2572.5 m^2/g, respectively. In contrast to MIL-101(Fe), NH_2−MIL-101(Fe) had larger surface area and higher catalytic performance groups (-NH_2). Therefore, the degradation rate of RhB by NH_2−MIL-101(Fe) exceeded 99% in 5 min, which was much higher than MIL-101(Fe) of 61.2% [34]. In addition, different organic linkers can be mixed to prepare MOFs with large specific surface area and used to selectively remove pollutants [45]. As shown in Fig. 3, UiO-66-n(COOH)$_2$ (n = 0, 0.25, 0.5, 0.75 and 1) was prepared by mixing 1,4-benzendicarboxylic acid (BDC) and 1,2,4,5-benzentetracarboxylic acid (BTC) ligands in different proportions for the selective removal and separation of RhB and MB [46]. With the increase in BTC content, the pore diameter and surface area decreased. This was attributed to the fact that the carboxylate group of BTC occupied the pores, reduce the surface area and the crystallinity of catalyst. Therefore, UiO-66–0.25(COOH)$_2$ showed the highest adsorption capacity for those samples of the RhB which is cationic dye with large size. To further examine the selective removal ability of these multivariate MOFs of UiO-66–0.25(COOH)$_2$ and UiO-66–0.75(COOH)$_2$, cationic dye MB and anionic dye methyl orange were tested. In the mixed dye wastewater, MB was quickly removed, which proved that UiO-66–0.25(COOH)$_2$ and UiO-66–0.75(COOH)$_2$ had the selective removal capacity of MB. The mechanism of this phenomenon was that the uncoordinated carboxylate groups on the TBC linkers made a negatively charged skeleton and negative surface potential of the MOF, which contribute to remove the cationic dye. Meanwhile, UiO-66–0.75(COOH)$_2$ had small pores and only allowed MB with small molecules to enter its skeleton.

The stability of the material is also closely related to the organic linking agent. PCN-134, which with two different topological linkers (4,4′,4′′-benzene-1,3,5-triyl-tris(benzoic acid) (H_3BTB) and tetrakis (4-carboxyphenyl) porphyrin (TCPP)), was synthetically achieved by Gao *et al.* [47]. As a mixed-linker Zr-MOFs, PCN-134 exhibits much improved stability compared to the 2D Zr-BTB, because the mixed-linker 3D structure increases the rigidity of the entire framework and further affects the stability of the material. Therefore, by designing MOFs with suitable organic linkers, the performance of catalysts can be further improved. And as shown in Table 1 [33,34,48-55], the difference of organic linkers will lead to great differences in the pore size, pore volume and specific surface area of the catalyst.

Table 1
Comparison of diameters, pore sizes and specific surface areas of MOFs with different organic ligands.

MOF	Temperature and time (°C, h)	Metal material	Organic ligand	Pore size (nm)	Pore volumes (cm^3/g)	Specific surface area (m^2/g)	Ref.
MIL-88B(Fe)	120, 12	$FeCl_3•6H_2O$	1,4-bezenedicarboxylic acid	1.78	0.191	994	[33]
MIL-101(Fe)	110, 24	$FeCl_3•6H_2O$	terephthalic acid	2.9	2.3	2122.6	[34]
NH_2−MIL-101(Fe)	110, 24	$FeCl_3•6H_2O$	2-aminoterephthalic acid	1.2–3.4	1.7	2572.3	
MIL-53(Fe)	150, 15	$FeCl_3•6H_2O$	terephthalic acid	2–5	0.24	367.99	[48]
MIL-88A(Fe)	70, 4	$FeCl_3•6H_2O$	fumaric acid	23.7	0.033	25.5	[49]
MIL-100(Fe)	150, 12	$FeCl_3•6H_2O$	1,3,5-benzenetricarboxylic acid	250–500	0.656	1271.91	[50]
MIL-101(Cr)	200, 12	$Cr(NO_3)_3•9H_2O$	1,4-benzenedicarboxylic	15–40	0.532	2452	[51]
MIL-101(Cr)-SO_3H	180, 144	$Cr(NO_3)_3•9H_2O$	monosodium 2-sulfoterephthalic acid	3.07	–	1545.4	[52]
UiO-66	120, 24	$ZrCl_4$	terephthalic acid	1.4	0.83	1335	[53]
UiO-67	120, 24	$ZrCl_4$	biphenyl-4,40-dicarboxylic acid	100	–	1638	[54]
Zr_6-BDC–NO_2	80, 24	$ZrOCl_2•8H_2O$	2-nitroterephthalic acid	0.6–1.2	–	960	[55]
Zr_6-BPDC-$(NO_2)_2$	80, 24		2,2′-nitro-4,4′-biphenyl dicarboxylic acid	1.2–2.2	–	1205	
Zr_6-fBDC	80, 24		2,3,5,6-tetrafluoro-1,4-benzenedicarboxylate	0.6–0.8	–	1021	
Zr_6-fBPDC	80, 24		2,2′,3,3′,5,5′,6,6′-octafluoro-4,4′-biphenyldicarboxylate	1.2–1.5	–	1148	

"-"means it is not mentioned in reference.

3. Synthesis methods

To prepare MOFs with excellent physical and chemical characteristics and improve the catalytic performance by changing their composition, structure and size, various methods such as hydrothermal method [45,52,56], sol-gel method [57–59], electrochemical method [60], microwave [61–63] and ultrasonic assisted synthesis method [47,64,65] and other emerging synthesis method have been developed and widely used.

3.1. Hydrothermal method

Hydrothermal method is the most popularly used for the synthesis of MOFs which react with soluble pre-products under high temperature and high pressure in a sealed space. The processed material is put into a pressurized autoclave, heated to cause polymerization reaction and obtain a precipitated material. The advantage of this method is easy operation and general applicability.

MIL-53(Fe) is usually obtained by heating at 150 °C for 15 h [38,48]. In order to improve the performance of the material, usually the prepared MIL-53(Fe) is mixed with other materials and then heated under high temperature and high pressure to obtain a derivative of MIL-53(Fe) or a modified catalyst. For instance, MIL-53(Fe) and $Bi(NO_3)_3•5H_2O$ were heated at 160 °C for 24 h to prepare MIL-53(Fe)/BiOCl composite [66]. However, MIL-53(Al) was synthesized by heating at 150 °C for 24 h [67]. Usually, the preparation pressure in MIL-101(Fe) was about 110 °C, and the reaction time was relatively short (20–24 h) [34,68,69]. However, for other MOFs, this method even takes a few days. Li *et al.* [24] synthesized NH_2−MIL-53(Al) by mixing the dissolved $AlCl_3•6H_2O$ and 2-aminoterephthalic acid into a reaction kettle, holding it at 130 °C for 72 h. MIL-100(Fe) also was heated at 130 °C for 72 h to be prepared [70]. Guo *et al.* [71] used 2-sulfo-terephthalic acid monosodium salt as the organic ligand and chromium oxide as the metal center, heated in a reactor at 180 °C for 6 days, and repeatedly washed with water and methanol to remove impurities, finally dried to obtain MIL-101(Cr)-SO_3H. Meanwhile, it can be clearly seen from Table 2 that the hydrothermal reaction takes a long time [72–76].

It is precisely because of the long preparation time (several days to several weeks), high energy consumption, high equipment requirements and poor safety performance of hydrothermal method that researchers have begun to develop some technologies of electrochemical, microwave and ultrasonic-assisted methods to shorten preparation time.

3.2. Electrochemical method

The advantages of electrochemical method include mild reaction conditions, special physical and chemical properties and relatively fast synthesis process. Electrochemical synthesis of MOFs is to produce metal ions or hydroxide anions through oxidation or reduction reaction by electrolysis [77]. These ions combine with ligands to deposit MOFs on conductive substrates. Therefore, electrolyte, organic ligands and electrochemical parameters affect the structure and composition of MOFs, which further affects the degradation of pollutants. Meantime, this method can improve the yield of MOFs. Kumar *et al.* [78] synthesized $Cu_3(BTC)_3$−MOF under constant voltage electrolysis (with keeping current varying to make voltage constant) for more than 2.5 h, and the Cu content of MOF (54%) was higher than the previously reported value (22%). Ji *et al.* [79] prepared Cu-MOF by electrochemical method, found and demonstrated that using different organic ligands were expected to have varied morphology. Besides, Cu-MOF synthesized by 1,3,5-benzenetricarboxylic acid owned better electrochemistry than that using 1,4-benzenedicarboxylic acid or 1,2,4,5-benzenetetracarboxylic acid. Arul *et al.* [80] made improvement on the basis of Ji's study [79], and obtained Cu-BTC MOF-carbon nanotubes with high conductivity by BTC. The above materials were all prepared by electrochemical deposition method, and materials were deposited on the surface of the electrolytic cell, which is of low efficiency.

Microplasma could also be used to synthesize MOFs efficiently. Wei *et al.* [60] prepared HKUST-1 using *N,N*-dimethyllformamide to dissolve $Cu(NO_3)_2$ and BTC as precursor solution, treated with microplasma cathode for 15 min. MOFs were also synthesized by dielectric barrier discharge plasma-assisted method. The high temperature in the channel and the partial superheating of the solution led to the rapid Ce-MOFs formation. This method needed a voltage generator, which generated non-thermal plasma between electrodes [81]. Therefore, relatively expensive equipment and complicated operation are shortcomings of this electrochemical method.

Table 2
Examples of MOFs synthesized by hydrothermal method.

MOF	Materials	Temperature and time (°C, h)	Topography	Ref.
MIL-88B(Fe)	$FeCl_3$•$6H_2O$, 1,4-benzenedicarboxylic	120, 12	spindle-shaped morphology	[33]
NH_2−MIL-88B(Fe)	$FeCl_3$•$6H_2O$, 2-aminoterephthalic acid	100,12	uniform hexagonal-shaped crystals	[41]
MIL-88A(Fe)	$FeCl_3$•$6H_2O$, fumaric acid	70, 4	rod-like structure	[49]
MIL-100(Fe)	Reduced iron powder, 1,3,5-benzenetricarboxylic acid	150, 24	unusual particle-assembled cluster structure	[50]
MIL-53(Fe)	$FeCl_3$•$6H_2O$, terephthalic acid	150, 12	rob-like structure	[66]
MIL-101(Fe)/TiO_2	$FeCl_3$•$6H_2O$, terephthalic acid, TiO_2	110, 20	the octahedral shape	[68]
MIL-101(Cr)-SO_3H	CrO_3, 2-sulfoterephthalic acid monosodium salt	180, 144	regular octahedron morphology particle	[71]
Co-doped MIL-53-NH_2	$FeCl_3$•$6H_2O$, $CoCl_3$•$6H_2O$, 2-aminoterephthalic acid	150, 24	–	[72]
MOF-derived $CoFe_2O_4$/Fe_2O_3	Co-doped MIL-53-NH_2	550, 4	yeast-shaped structure	
g-C_3N_4@$CoFe_2O_4$/Fe_2O_3	Melamine, MOF-derived $CoFe_2O_4$/Fe_2O_3	550, 4	irregular massive structure	
MIL-101(Fe)	$FeCl_3$•$6H_2O$, terephthalic acid	110, 20	collapsed concave octahedron morphology	[73]
GO@MIL-101(Fe)	$FeCl_3$•$6H_2O$, terephthalic acid, GO	120, 24	1.0–2.0 μm polyhedron shape	[74]
MIL-101(Fe)	$FeCl_3$•$6H_2O$, acetic acid, 1,4-benzenedicarboxylic acid	110, 24	hexahedron shape	[75]
C-NH_2−MIL-101(Fe)	$FeCl_3$•$6H_2O$, acetic acid, 2-aminoterephthalic acid	110, 24	rod-like structure	
MIL-125(Ti)	tetrabutyl titanate, 1,4-benzenedicarboxylic acid	150, 48	smooth regular disk	[75]
BUC-21(Fe)	$FeSO_4$•$7H_2O$, 1,3-dibenzyl-2-imidazolidone-4,5-dicarboxylic acid, 4,4′-bipyridine	160, 72	rough sheet morphology	[76]

3.3. Sol-gel method

The raw material in sol-gel method is first treated for a liquid state, and highly active components that act as precursors are fully mixed in the liquid phase; then, the solution mixed with a metal salt solution and undergo chemical reactions such as hydrolysis or condensation to form sol system; the sol particles of the system polymerized slowly to form a gel with network structure; the gels were dried and sintered to obtain gelatin porous materials [57,58,82,83].

Mehta *et al.* [61] dissolved $Zn(NO_3)_2$•$6H_2O$ and 2-methylimidazole ($C_4H_6N_2$) in ethanol, respectively. After the two liquids were mixed, stirred at room temperature for 15 min, and centrifugation, washing, drying, and grinding, NP@$_{mono}$ZIF-8 was obtained. Cu/SiO_2−MOF was synthesized by two steps. Cu-MOF as precursor was heated to synthesize, then further fixed *in situ* in the silica carrier by sol-gel method [83]. However, this indirect synthesis method is complicated to operate and takes a long time.

The advantages of sol-gel method are low cost and relatively mild reaction conditions. However, sol and gel must be produced in the composite solution during the synthesis process. Because some solutions can not form sol-gel state (the size of dispersed particles in solution should be between 1 nm and 1000 nm, and the sol-gel solution also needs to aggregate to form solid state gel with network structure), therefore, there are limitations in the preparation of MOF materials by this method.

3.4. Emerging synthesis method

Emerging synthesis methods include microwave-assisted method, ultrasound-assisted method and mechanochemistry method, *etc.*

Both microwave-assisted method and ultrasound-assisted method are utilized to save the experimental time, make the crystals nucleate rapidly. For example, both MIL-140A and MIL-140B were synthesized at temperature of 220 °C by solvothermal method, which took 16 and 6 h, respectively. However, microwave heating only spent 17 min [84]. Also, using hydrothermal method to prepare CPM-5 needed 5 days, and only 10 min was needed by microwave-assisted heating [61]. In addition, due to the simultaneous nucleation of all crystals in the solution, the microwave method also makes the formation of nano-products with more uniform and smaller particle size [85]. In the C–NH_2−MIL-101 sample which was synthesized by traditional solvothermal, the number of particles with a size diversity of 200–600 nm was observed. Compared with the samples prepared by the traditional solvothermal method, the MW-NH_2−MIL-101 sample obtained by the microwave-assisted method had a smaller particle size of 150–250 nm [75]. Moreover, through manipulating reaction condition, the size and shape of the crystals can be varied [86]. The reaction time can be found from Table 3. The size and distribution of crystals increased from the irradiation time, eventually allowing particles with high surface area to be separated out. Meanwhile, reaction times affect the particle size of MOFs. As can be seen from Table 3, the microwave heating synthesis method has greatly prospered the design and preparation of MOFs. Meanwhile, this technology also has several outstanding advantages: It accelerates the reaction speed and greatly shortens the reaction time; the material with a high absorption rate has a significant purity and phase selectivity in some cases; and from microcrystals to nanoparticles, the real possibility of controlling crystal size is achieved; a compact synthesis device with low energy consumption can be used, while generating a small amount of chemical waste [87–89].

Ultrasound assistance can shorten reactions time that has been increasingly used in the last decades [90]. Besides, the high yields and mild conditions are also its advantages [47]. The high frequency of ultrasonic waves is used to make liquid molecules violently vibrate to generate holes, and then collide with synthetic materials. In the continuous collision and extrusion, chemical reactions occur to the raw materials, thereby synthesizing various MOFs [91]. However, this method is rarely used in the synthesis of materials, and is usually used as a raw material processing method, rather than a separate synthetic material. Therefore, the ultrasonic method is usually used in combination with other methods. For

Table 3
Microwave-assisted and other method preparation of MOFs.

MOF	Methods and parameters	Materials	Time (min)	BET surface area (m^2/g)	Micropore volume (cm^3/g)	Ref.
CPM-5	MW-hydrothermal, 150 °C, 300 W	$In(NO_3)_3$•xH_2O, 1,3,5-benzenetricarboxylic acid	5	1736	–	[61]
			10	2187	–	
	MW-hydrothermal, 150 °C, 100 W		10	1365	–	
	Hydrothermal, 120 °C		7200	686	–	
MW-MIL-101(Fe)	MW-hydrothermal, 110 °C	$FeCl_3$•$6H_2O$, 1,4-benzenedicarboxylic acid	45	383	2.9	[75]
C-MIL-101(Fe)	Solvothermal, 110 °C		1440	309	2.3	
MW–NH_2–MIL-101(Fe)	MW-hydrothermal, 110 °C	$FeCl_3$•$6H_2O$, 2-aminoterephthalic acid	45	258	2.2	
C-NH_2–MIL-101(Fe)	Solvothermal, 110 °C		1440	239	1.7	
MIL-140A-NH_2–MW	MW-hydrothermal, 220 °C	$ZrCl_4$, 2-amino-1,4-benzenedicarboxylic acid	17	234	–	[84]
MIL-140A-MW		$ZrCl_4$, 1,4-benzenedicarboxylic acid	17	337	–	
MIL-140A-CE	Solvothermal, 220 °C		960	585	–	
MIL-140B-MW	MW-hydrothermal, 220 °C	$ZrCl_4$, 2,6-naphthalenedicarboxylic acid	17	438	–	
MIL-140B-CE	Solvothermal, 220 °C		360	398	–	
MOF-5	MW-hydrothermal, room temperature, 90 W	$Zn(NO_3)_2$•$6H_2O$, terephthalic acid	2	1203	2.17	[87]
MW-MIL-101(Cr)	MW-hydrothermal, 210 °C, 400 W	$CrCl_3$•$6H_2O$, terephthalic acid	15	3071	1.51	[88]
			60	3196	1.55	
MIL-101(Cr)	Hydrothermal, 210 °C		360	2735	1.43	
			1440	3160	1.54	

example, to ensure uniform solution, Wan *et al.* [64] sonicated the mixed solution of $FeSO_4$•$7H_2O$ and H_3BDC for 20 min, and synthesized MIL-100(Fe)-MW after 90 min under microwave radiation. Burgaz *et al.* [62] utilized consecutive combination of ultrasound and MW method to synthesize MOF-5. The SEM images of MOF-5 that was synthesized by using MW method with no ultrasound treatment resulted in micron-sized MOF-5 crystals (3–10 μm) with some unidentified impurities. Using ultrasound and MW method had 20–80 nm of sizes and 95% of yields.

Mechanochemical synthesis is a method in which reagents produce chemical reactions through mechanical forces to synthesize materials [92]. Compared with other methods, this method is a greener synthesis process, due to synthesize MOFs with little or no solvent. Ali-Moussa *et al.* [93] synthesized two Zr-based MOFs, UiO-67 and its dipyridyl analogue (UiO-67-bpy) by ball milling. However, due to the low crystallinity of the material, its specific surface areas were 750 m^2/L and 650 m^2/L respectively, far lower than the expected value of 3000 m^2/L. Moreover, Kong *et al.* [58] prepared ZIF-8 by solvothermal, stirring and ball milling methods, respectively. Through characterization, the BET surface area of ZIF-8 synthesized by hydrothermal method (1390 m^2/g) and stirring method (1220 m^2/g) was similar, and that of ZIF-8 prepared by ball milling method (916 m^2/g) was significantly lower than that of other methods. Therefore, the mechanochemical method produces less waste and environmental protection, but the disadvantages of low crystallinity of the prepared materials and the need for special synthesis equipment make the application scope of this method lower than that of hydrothermal method.

4. Application of MOFs in AOPs and catalytic mechanism

4.1. Fenton-like oxidation

Fenton progress is that Fe^{2+} catalyzes H_2O_2 to produce $^{\bullet}OH$ to oxidize organic pollutants into small molecular substances. Although this method has advantages of simple equipment, convenient operation and low cost, it has obvious shortcomings of narrow pH range and secondary pollution to water which caused by easily leached iron ions [94–97]. Therefore, Fenton-like process is developed on the basis of Fenton progress. The mechanism of Fenton-like method to expand the reaction pH range is that substances such as light, electricity and persulfate activate the regeneration of hydroxide complex (iron sludge) to form Fe^{2+}, and the generation of some acidic substances in the reaction process reduces the pH of the solution [98].

Among the various types of MOFs applied to Fenton-like, Fe-based MOFs as heterogeneous Fenton-like catalysts have great potential [99,100]. NH_2–MIL-101(Fe) synthesized by Taha *et al.* [34], which completely removed 0.25 mmol/L RhB in the pH range of 3.1–11 within 10 min, and its performance was much better than the Fenton progress removing pollutants in the pH range of 4–6. Moreover, although MIL-100(Fe) is also successfully used as a Fenton-like catalyst, pure MIL-100(Fe) has low catalytic activity and lack of coordination, it still needs improvement. Due to synergistic catalytic action of Fe(II) and Fe(III) ions accelerated the production of $^{\bullet}OH$, adding Fe(II) to MIL-100(Fe) to synthesize Fe^{II}@MIL-100(Fe) could improve the catalytic efficiency and mineralization ability [101]. However, in Fenton-like progress, a noteworthy issue is that the leaching of metal ions. The leaching experiments found that Fe(II) ions supported on MIL-100(Fe) could be dissolved into the solution, and the concentration of elemental iron leached from Fe^{II}@MIL-100(Fe) could reach to 7.1 mg/L, which was far higher than the environmental standard (2 mg/L, established by the European Union) [101]. In addition, the leaching concentration of metal ions in MOF materials with bimetallic centers is also serious. It was detected in the solution that the leaching concentration of Fe in iron-copper bimetallic organic framework material (Fe_xCu_{1-x}(BDC)) reached 7.23 mg/L, and the leaching concentration of Cu was 0.11 mg/L [36]. The reason for the leaching of metal ions may be that the metal active sites are loaded on the surface of the catalyst, and the combination with the organic ligands is not tight, which causes the metal ions to fall off easily into solution, and bimetallic interweaving can easily cause the pores of MOF material to be collapsed. Therefore, further researches have been conducted about MOFs modification to improve their catalytic activity and reduce the leaching rate of metal ions. Tang *et al.* [37] obtained three-dimensional flower-shaped MOF FeCu@C as Fenton-like catalyst based on the iron-copper bimetallic organic framework material after calcination under high temperature, and the copper leaching rate reached to 3.34 mg/L.

In contrast, the metal leaching rate of MOFs catalysts with single metal centers is much low. For example, the maximum concentration of iron ions leached in phenol degradation by MIL-88B(Fe) was only 0.68 mg/L, which was much lower than that of other MOF materials which with bimetallic centers [102]. Tang *et al.* [50] coordinated unsaturated iron center metal organic framework material

CUS-MIL-100(Fe) with mixed Fe^{II}/Fe^{III} could degrade SMT almost 100% within 180 min. Though the activity of the catalyst decreased slightly after repeated five times, the highest leaching concentration of iron ions in the solution was 0.41 mg/L, that was much lower than using Fe^{II} loaded on MIL-100(Fe) (Fe^{II}@MIL-100(Fe)) [101] and bimetal MOFs [36,37]. And the morphology, crystal structure, functional group and catalytic activity of activated CUS-MIL-100(Fe) under vacuum conditions were similar as the fresh catalyst. The degradation mechanism of such Fenton-like MOFs catalyst is that the adsorbed H_2O_2 on the surface of the catalyst was rapidly decomposed by the change and conversion of iron valence, and thereby enhancing the catalytic activity and degradation efficiency. Therefore, enhancing the tight bonding between organic ligands and metals is an effective method to improve the stability of materials and reduce the leaching rate of metal ions.

In addition to iron-based catalysts, other redox states of chromium, cerium, copper, cobalt, manganese, and ruthenium can also be selected as Fenton-like catalysts. And the Fenton-like systems which with Cu(II) catalysts have attracted increasing attentions. Comparing with the Fe(III)-based catalysts, the Cu(II) in H_2O_2 system exhibited the advantages of high efficiency [103,104], wide adaptability to temperature and pH [105,106]. Using Cu-MOF as templates and precursors, Xiong *et al.* [107] prepared Cu_xO/C composite materials with CuO and Cu_2O nanoparticles to degrade RhB through two chemical reactions. After adding H_2O_2, the degradation rate of RhB reached above 98%. Wu and coworkers constructed MIL-100(Fe)/CoS to degrade 99.2% 10 mg/L bisphenol A [36]. The study found that the Fe-S bond formed at the interface of the two components promote Fe^{3+}/Fe^{2+} cycle by increasing the electron mobility (Co to Fe and S to Fe), this is the first time that the Fe^{3+}/Fe^{2+} cycle in Fe-MOF has been explained by studying Fe-MOF/MSx interface interaction in Fenton-like progress.

Photo-Fenton degrades pollutants by reducing Fe^{3+} and photolysing H_2O_2 to generate $^{\bullet}OH$. Tang *et al.* [108] synthesized a series of iron-based metal organic frameworks (Fe-MOF) to degrade hydrochloride tetracycline. To increase the visible light absorption of the iron-based MOF, Nguyen *et al.* [109] introduced another metal to prepare bimetallic organic framework of Al/Fe-MOF and MIL-88B(Fe) as a photo-Fenton catalyst. In the characterization test, it was found that the specific surface area of Al/Fe-MOF and MIL-88B(Fe) were 285 m^2/g and 47 m^2/g, and the pore sizes were 1.5 nm and 1.9 nm, respectively. Within 120 min, the degradation rate of RhB which using MIL-88B(Fe) was 83%, while that using Al/Fe-MOF could exceed 96%. This study demonstrated that the larger specific surface area allows MOFs have more active sites, coupled with the transition of the bimetallic charge, and therefore the catalytic efficiency could be significantly enhanced.

In addition, electro-Fenton process also could generate a large amount of $^{\bullet}OH$ and other strong oxidants in bulk solution. Compared with the decomposition of H_2O_2 to generate $^{\bullet}OH$, the reduction of O_2 in the cathode reaction to generate $^{\bullet}OH$ is safer, cheaper and more environmentally friendly [110]. Ye *et al.* [111] obtained nano-ZVI@CN by calcining NH_2-MIL(Fe) under N_2, and used nano-ZVI@CN as a catalyst to treat the gemfibrozil in the electric-Fenton process with a high removal rate of 100%. The H_2O_2 produced at the cathode undergoes a heterogeneous Fenton reaction to Fe(II) on the catalyst surface, producing $^{\bullet}OH$ and iron ions. In addition, the active chlorine and $^{\bullet}OH$ generated by the anode reaction will also degrade pollutants. And the nano-ZVI and Fe_3O_4 nanoparticles present in the rod ensure the supply of Fe(II)/Fe(III), and nano-ZVI was the main element responsible for the continuous regeneration of Fe(II). Meantime, the presence of N-doped porous carbon promoted the electron transfer. The method to increase the active oxide species in the solution is to increase the catalytic center of MOFs. Zhou *et al.* [112] used Mn-doped MIL-53(Fe) as a precursor to successfully synthesize Mn/Fe@PC catalyst after carbonization of MOF, which was used as catalyst in electro-Fenton process to degrade triclosan Mn/Fe@PC–CP showed high catalytic performance and stability, triclosan could be completely degraded within 120 min, and TOC removal reached 56.9% ± 2.0% within 240 min. The reason was that dispersion of the active sites of $Fe^{II}/{\equiv}Mn^{II/III}$ obviously promoted the formation of H_2O_2 and ultimately promote the degradation of triclosan, and the conversion between ions reduced the ion leaching rate [112].

4.2. Photocatalysis

As a low-cost and environmentally friendly technology, photocatalysis has shown significant potential for water pollution purification. MIL-53(Fe) composed of Fe(III) and 1,4-benzenedicarboxylic acid is also commonly used in photocatalyst due to its high response to visible light response area. Nevertheless, owing to the rapid recombination of electron-hole pairs, scholars have made many attempts to overcome this drawback. In the research by Chen *et al.* [113], the MIL-53(Fe) with mixed valence Fe metal centers formed under vacuum inert gas exhibited considerable photocatalytic performance. It could degrade 96.28% and 95.01% of 20 mg/L RhB and hydrochloride tetracycline, which was 1.13 and 1.33 times higher than that of MIL-air53(Fe) prepared in air, because the charge migration in the mixed valence Fe^{II}/Fe^{III} chains reduced h^+-e^- pairs. Jiang *et al.* [114] prepared photocatalysts with core-shell structure ZnO@ZIF-8. Its catalytic performance was 40% higher than that of ZnO, because the core-shell structure increased the active sites. Zhang *et al.* [115] synthesized a new type of absorptive photocatalysis TiO_2/mag-MIL-101(Cr) with tetrabutyl titanate and magnetic MIL-101(Cr). 0.5 g/L TiO_2/mag-MIL-101(Cr) could completely remove 20 mg/L bisphenol F, and the removal rate of acid red 1 was 90%. In addition, Miao *et al.* [66] used BiOCl to anchor the surface of MOF-53(Fe) for synthesizing MIL-53(Fe)/BiOCl, in that the photoelectrons were accumulated on the BiOCl with lower conduction band (CB) while the holes stored on the valence band (VB) of MIL-53(Fe). Therefore, the key of improving photocatalytic efficiency of MOFs is to reduce the rapid recombination rate of electron-hole pairs.

Manufacturing heterojunction is also a method to realize the effective separation and transfer of light-excited electron and hole charge. The composite of UiO-66-NH_2 and Cu_2O to obtain UiO-66-NH_2/Cu_2O with heterojunction was superior to pure Cu_2O and UiO-66-NH_2 in the photocatalytic degradation of methyl orange [116]. The composite material obtained by coupling carbonitride carbon (g-C_3N_4) with unique crystal structure and visible light responsiveness to MOFs will also form a heterojunction that facilitates the separation of electron-hole pairs to improve photocatalytic activity [117]. For example, Zhang *et al.* [53] used g-C_3N_4/UiO-66 nanohybrids CNUO as photocatalyst, and found that the addition of g-C_3N_4 improved the pore size of CNUO, and $O_2^{\bullet-}$ was formed by photo-generated electron of UiO-66 which improved the degradation rate of RhB. Moreover, Huang *et al.* [118] fabricated the protonated g-C_3N_4 coated with MIL-100(Fe), which denitrified and oxidized the pyridine of RhB by molecular oxygen. He *et al.* [68] used MIL-101(Fe) and TiO_2 to synthesize the magnetic MIL-101(Fe)/TiO_2 composite material, which removed 92.76% of tetracycline in 10 min under visible light, which was 2.3 times than that of pure MIL-101(Fe). Hejazi *et al.* [70] used TiO_2 and MIL-100(Fe) to construct a heterojunction TiO_2@MIL-100(Fe) to degrade MB with a high degradation rate of 100%, in which that the mineralization rate could reach 87%. The heterojunction between semiconductors and MOFs in the composite has a synergistic effect, and the effective interface charge transfer improved the separation effect of photo-induced electron-hole pairs, and improve the absorption of visible light by reducing band gap.

The energy-saving advantages of photocatalytic reaction make it widely concerned in the field of wastewater treatment. However, its shortcomings are also very obvious. Under normal circumstances, the photocatalytic reaction takes a long time of 1–3 h, and large number of impurities in the water will greatly affect the catalytic efficiency. Therefore, the practical application of photocatalyst needs further research.

4.3. Ozone catalysis oxidation

The disadvantages of ozone catalytic oxidation are low ozone utilization and TOC removal rate. Therefore, using MOFs to overcome those shortcomings are necessary. Yu *et al.* [44] studied and compared four MOFs (MIL-53(Fe), MIL-88B(Fe), MIL-100(Fe) and MIL-101(Fe)) to catalyze ozone for RhB degradation. MIL-53(Fe) showed the highest removal efficiency in catalytic ozonation process, that could shorten the degradation times from 10 min (only ozone treatment) to 2.5 min to achieve complete degradation, and a TOC removal rate was nearly 40% at 30 min. Capture experiments and active site detection showed that the Lewis acid sites (LAS) on the surface of MOFs were active sites for catalytic ozonation, which could promote the decomposition of ozone into reactive oxide species (ROS). Besides, the mechanism of photocatalytic ozone oxidation technology was also proposed to degrade 4-nitrophenol [119]. MIL-88A(Fe) produced conduction band e^- and h^+ in the CB and VB under UV (254 nm) radiation. And the CB electrons were transferred to ozone to reduce charge carrier recombination and catalytically decompose O_3 to generate more ROS on the LAS of MIL-88A(Fe) for 4-nitrophenol degradation and mineralization. Therefore, the TOC removal rate (75%) of 4-nitrophenol in this system was much higher than that of photocatalysis (17.6%) and catalytic ozonation (38.7%) [119].

Material modification is an effective way to enhance O_3 decomposition to produce $^{\bullet}OH$. MOFs of ZIF-67-derived Co_3O_4–C@FeOOH composite was used as an efficient catalyst for norfloxacin degradation by ozonation [120]. ZIF-67 was used as precursor and heated treatment to obtain Co_3O_4-carbon. Through modification by FOOH, which was wrapped on Co_3O_4-carbon to prepare MOF-derived Co_3O_4-carbon composite material. The specific surface area of the formed composite was about 2.5 times that of Co_3O_4-C, which provided active sites for catalytic O_3 decomposition, enhanced the generation of $^{\bullet}OH$ and TOC removal rate. The coexistence of Fe and Co in various valence states in catalyst improved the conversion of Co^{III}/Co^{II} and Fe^{III}/Fe^{II}, which would increase the catalytic activity in catalytic ozonation process.

4.4. Persulfate catalysis

$SO_4^{\bullet-}$ has a strong oxidation potential (2.6 V) with wider pH range than $^{\bullet}OH$, meanwhile generate less disinfection by-products in oxidation process [69]. Heating, UV irradiation, homogeneous transition metal catalysis and heterogeneous photocatalysis are common activating methods for sulfate radical AOPs [121].

Wan *et al.* [64] added the regulator CH_3COOH to obtain MIL-100, used to activate persulfate (PS) to degrade orange G. In addition, through the predicting the reaction site by frontier molecular orbital theory and dual descriptor method, it was found that the degradation pathway of orange G was attacking $N_2{=}N_2$ of aromatic ring hydroxyl groups by $SO_4^{\bullet-}$ and $O_2^{\bullet-}$ to form hydrolyzed phenol substitutes and finally mineralize the pollutant [64]. Wu *et al.* [122] encapsulated ZIF-67 with Fe_3O_4 as the core in ZIF-8. The electron transfer between Fe_3O_4 and cobalt active center activated PS to produce $SO_4^{\bullet-}$, which can completely remove 5 mg/L carbamazepine within 30 min.

Yi and colleagues prepared PDINH/MIL-88A(Fe) with perylene-3,4,9,10-tetracarboxylic diimide as raw materials to remove 95.7% of chloroquine phosphate by activating PS under low power LED visible light [123]. Studies had shown that the efficient removal rate was mainly attributed to the production of different active species ($SO_4^{\bullet-}$, $^{\bullet}OH$, $O_2^{\bullet-}$, h^+ and $^1O_2$) through direct and indirect activation of activating PS. Moreover, Wang *et al.* [124] fixed MIL-88A(Fe) on cotton fiber to prepare MIL-88A(Fe)/cotton fibers activated PS to produce $SO_4^{\bullet-}$ and $^{\bullet}OH$ under UV radiation. Through quantitative structure-activity analysis, it was found that tetracycline antibiotics were transformed into corresponding intermediates with low toxicity within 8 min. Liao *et al.* [125] synthesized surface-oriented MIL-88B-Fe with rod-like structure based on benzoic acid functionalized g-C_3N_4 and MIL-88B-Fe, which removed 95% RhB in 60 min, with PS as oxidant. Gong *et al.* respectively designed MOFs based on nitrogen-doped carbon, using MIL-101(Fe) and ZIF-CN (ZIF-CN was obtained by carbonizing ZIF-8) as template to obtain g-C_3N_4/MIL-101(Fe) and ZIF-CN/g-C_3N_4 at high temperature [69]. The SEM image showed that the shape of ZIF-NC was rhombic dodecahedron, about 200 nm of the size. ZIF-CN/g-C_3N_4 activated PMS under visible light (Vis) irradiation, the degradation rate of BPA (20 mg/L) reached 97% within 60 min. The g-C_3N_4/MIL-101(Fe) had an octahedral structure with a particle size range of 0.5–2 μm. In g-C_3N_4/MIL-101(Fe)/Vis/PS system, BPA (10 mg/L) could be removed 98% within 60 min. In both experiments, ethylenediaminetetraacetic acid disodium salt, *p*-benzoquinone, *n*-butanol and methanol were used to quench active radicals. It was found that two free radicals of $O_2^{\bullet-}$ and h^+ played major roles in BPA degradation by ZIF-NC/g-C_3N_4. In g-C_3N_4/MIL-101(Fe)/Vis/PS system, $SO_4^{\bullet-}$, h^+ and $O_2^{\bullet-}$ were major ROS. Moreover, Lv *et al.* [1] used MOF and COF to form a new type of MOF@COFs hybrid material, as an effective photocatalyst, combined with advanced sulfate-based oxidation process, which removed BPA about 99%.

Hu *et al.* [126] prepared MIL-101(Fe) to degrade tris(2-chloroethyl) phosphate (TCEP). The mechanism of photocatalysis reaction on MIL-101(Fe) was transformation of Fe(III) to Fe(II) under visible light which further induced transformation of $S_2O_8^{2-}$ to $SO_4^{\bullet-}$ and produced $^{\bullet}OH$ to oxide TCEP. Zhang *et al.* [127] utilized $FeCl_3{\bullet}6H_2O$ and 2-aminoterephthalic acid to synthesize MIL-101-NH_2 to activate oxone and degrade acid azo dye amaranth completely. In this process, amine groups absorbed visible light and transferred electrons to the Fe-O clusters on MIL-101-NH_2 to generate $^{\bullet}OH$ and $SO_4^{\bullet-}$, and thereby greatly improving the degradation efficiency of azo dye amaranth. Moreover, Lu *et al.* [72] synthesized a new type of composite material g-C_3N_4@$CoFe_2O_4$/Fe_2O_3 by hydrothermal method and calcination, and then used the resulting hybrid photocatalyst as a high-efficiency mediator to activate PS under visible light. The heterojunction formed between the MOF-derived $CoFe_2O_4$/Fe_2O_3 and g-C_3N_4 could effectively inhibit the recombination of photo-induced electrons and holes. Meanwhile, doping a small amount of MOF-derived $CoFe_2O_4$/Fe_2O_3 significantly increased visible light absorption capacity of g-C_3N_4 and reduced the band gap of g-C_3N_4, effectively improving the catalytic efficiency. Within 80 min, tetracycline of 99.7%, BPA of 98.1%, SMX of 94.8%, diclofenac sodium of 97.0%, ibuprofen of 96.1% and ofloxacin of 96.5% were removed [72].

In addition, it is also possible to synthesize a core-shell structured MOFs for increasing the reactive sites of the material to improve the catalytic performance. Zhu *et al.* [128] utilized ZIF-67@GN and thioacetamide to synthesize Co_3S_4@GN. After calcination, a reactive shell CoS@GN with a large number of exposed active sites was obtained, which activated peroxymonosulfate to degrade 100% of BPA within 8 min.

4.5. Application of MOFs in other methods

In addition to the oxidation techniques summarized above, MOFs have also been applied in some new developed physical field assisted AOPs. Sisi *et al.* [129] synthesized MOF-2 nanomaterials, which was used to compare the degradation rate of dye acid blue 7 in six water treatment processes including sonolysis, adsorption, peroxydisulfate ($S_2O_8^{2-}$), sono-activated peroxydisulfate ($US/S_2O_8^{2-}$), sonocatalytic process using MOF-2 (US/MOF-2) and sonocatalytic process using MOF-2 in the presence of peroxydisulfate ($US/MOF\text{-}2/S_2O_8^{2-}$). After 60 min of each individual process, the results showed that $US/MOF\text{-}2/S_2O_8^{2-}$ had the highest degradation efficiency, which can remove 76.44% of the dye acid blue 7. The reason was that ultrasound promoted the activation of PS by the catalyst and lead to accelerating the production of various free radicals ($^{\bullet}OH$, $SO_4^{\bullet-}$, $O_2^{\bullet-}$ and $^1O_2$) [129].

Moreover, electrochemical AOPs under gamma ray radiation also accelerate iron-based MOFs to produce ROS to decompose antibiotics. In the study of ionizing radiation-induced catalytic degradation of antibiotic wastewater, the TOC removal rate of cephalosporin C and SMT were 20.2% and 4.5% by γ-irradiation alone (3.6×10^{14} Bq of radioactivity). After adding Fe/C nanomaterials (DMOFs) carbonized with MIL-100(Fe) as the precursor, the TOC removal rate of cephalosporin C and SMT increased to around 42% and 51%, and degradation rate of them were raised by 1.3 times and 1.8 times [130].

5. Conclusions and outlook

In this review, the recent progresses of MOFs applied in AOPs for emerging organic contaminants degradation were summarized. The multifunctional sites introduced into MOFs through changing the metal center and organic framework, could realize selective removal of structurally diverse pollutants. Besides, another pathway is to dope other materials from MOF precursor to offer more opportunities for catalysis reaction.

Though MOFs are competitive for degradation of emerging pollutants, some challenges of reusability and stability should be solved to achieve multicycle and large-scale application, due to leaching of metal ions and recovery of brittleness powdered catalysts are difficult to fully maintain their functions and critical structure. Fixing it on a stent or plating it on a biofilm is a potential solution, despite that metal leaching is still unavoidable. Lack of treating actual wastewater is another challenge, as of most studies are conducted under simulated wastewater. Therefore, it is urgent to study the catalytic performance and stability in the actual wastewater which the situation will be more complicated. Another issue is selection of economically viable and environmental-friendly organic ligands to decrease the cost of MOFs preparation. With the continuous efforts on these worthy improvements, more high-performance MOFs would be provided and generate a large impact on the wastewater treatment.

Declaration of competing interest

All authors declared that they do not have any commercial and associative interests that represent a conflict of interest in connection with the other work submitted.

Acknowledgments

The work was supported by the National Natural Science Foundation of China (Nos. 21906088, 51902169, 52170039), the National Science Foundation for Post-doctoral Scientists of China (No. 2021T140165), the Heilongjiang Provincial Natural Science Foundation of China (No. LH2020B023), Department of Education Heilongjiang Province (Nos. 135309338, 135309351), University Nursing Program for Young Scholars with Creative Talents in Heilongjiang Province (Nos. UNPYSCT-2020068, UNPYSCT-2020067).

References

[1] S.W. Lv, J.M. Liu, C.Y. Li, et al., Chemosphere 243 (2019) 125378.
[2] S. Esplugas, D.M. Bila, L.G.T. Krause, M. Dezotti, J. Hazard. Mater. 149 (2007) 631–642.
[3] S. Wang, L. Li, S. Yu, et al., Chem. Eng. J. 406 (2020) 126722.
[4] S. Valizadeh, S.S. Lee, K. Baek, et al., Environ. Res. 200 (2021) 111757.
[5] Q. Yang, H. Hong, Y. Luo, Chem. Eng. J. 392 (2020) 123680.
[6] K. Roy, V.S. Moholkar, Chem. Eng. J. 386 (2020) 121294.
[7] B.E. Meteku, J. Huang, J. Zeng, S. Aslam, Z. Yan, Chin. Chem. Lett. 32 (2021) 3245–3251.
[8] Y.L. Tong, H.Q. Liu, M.Z. Dai, L. Xiao, X. Wu, Chin. Chem. Lett. 31 (2020) 2295–2299.
[9] H. Lin, J. Niu, J. Xu, Y. Li, Y. Pan, Electrochim. Acta 97 (2013) 167–174.
[10] D. Huang, G. Wang, M. Cheng, et al., Chem. Eng. J. 412 (2021) 127817.
[11] Y. Li, W. Zhang, J. Niu, Y. Chen, Environ. Sci. Technol. 47 (2013) 10293–10301.
[12] O.M. Yaghi, G. Li, H. Li, Nature 378 (1995) 703–706.
[13] H.L. Li, M.M. Eddaoudi, M. O'Keeffe, O.M. Yaghi, Nature 402 (1999) 276–279.
[14] Y.T. Qin, Y. Wan, J. Guo, M.T. Zhao, Chin. Chem. Lett. 33 (2022) 693–702.
[15] C.W. Ding, W. Luo, J.Y. Zhou, et al., ACS Appl. Mater. Interfaces 11 (2019) 45621–45628.
[16] Y. Song, X. Xin, S. Guo, et al., Chem. Eng. J. 384 (2020) 123337.
[17] J. Cao, X. Li, X. Wang, et al., Chem. Eng. J. 384 (2020) 123363.
[18] L.K. Macreadie, R. Babarao, C.J. Setter, et al., Angew. Chem. 132 (2020) 6146–6154.
[19] M. Suyetin, M.V. Peskov, U. Schwingenschlögl, Chem. Eng. J. 384 (2020) 123296.
[20] J.A. Cruz-Navarro, F. Hernandez-Garcia, G.A.A. Romero, Coordin. Chem. Rev. 412 (2020) 213263.
[21] D. Yang, B.C. Gates, ACS Catal. 9 (2019) 1779–1798.
[22] F. Wang, H.F. Fu, F.X. Wang, et al., J. Hazard. Mater. 423 (2022) 126998.
[23] Y.X. Li, C.C. Wang, H. Fu, P. Wang, J. Environ. Chem. Eng. 9 (2021) 105451.
[24] H.F. Fu, C.C. Wang, W. Liu, Chin. Chem. Lett. 33 (2022) 1647–1649.
[25] H.L. Jiang, Q.H. Yang, C. Chuen, C.H. Lin, Angew. Chem. Int. Ed. 58 (2018) 3511–3515.
[26] I.A. Ibarra, E. Lima, V. Jancik, et al., J. Mater. Chem. A 8 (2020) 12345–12349.
[27] M. Zhu, Y. Liu, M. Chen, et al., Chin. Chem. Lett. 31 (2020) 2683–2688.
[28] Y.S. Kang, Y. Lu, K. Chen, et al., Coordin. Chem. Rev. 378 (2019) 262–280.
[29] C.Q. Cui, G.D. Li, Z.Y. Tang, Chin. Chem. Lett. 32 (2021) 3307–3321.
[30] J. You, C. Zhang, Z. Wu, Z. Ao, B. Lai, Chem. Eng. J. 415 (2021) 128890.
[31] T. Hu, F. Deng, H. Feng, et al., Appl. Mater. Today 24 (2021) 101161.
[32] D.X. Ma, B.Y. Li, Z. Shi, Chin. Chem. Lett. 29 (2018) 827–830.
[33] M. Ahmad, X. Quan, S. Chen, H. Yu, Appl. Catal. B: Environ. 264 (2020) 118534.
[34] A.A. Taha, L. Huang, S. Ramakrishna, Y. Liu, J. Water Process Eng. 33 (2020) 101004.
[35] A. Kirchon, P. Zhang, J. Li, et al., ACS Appl. Mater. Interfaces 12 (2020) 9292–9299.
[36] J.T. Tang, J.L. Wang, Chemosphere 241 (2020) 125002.
[37] J.T. Tang, J.L. Wang, Chem. Eng. J. 375 (2019) 122007.
[38] L. Xie, Z. Yang, W. Xiong, et al., Appl. Surf. Sci. 465 (2018) 103–115.
[39] D. Liu, M. Li, X. Li, F. Ren, L. Zhou, Chem. Eng. J. 387 (2020) 124008.
[40] J.J. Du, X. Zhang, X.P. Zhou, D. Li, Inorg. Chem. Front. 5 (2018) 2772–2776.
[41] Y.X. Wang, Z. Zhong, Y. Muhammad, et al., Chem. Eng. J. 398 (2020) 125684.
[42] J.H. Cavka, S. Jakobsen, U. Olsbye, et al., Chem. Soc. 130 (2008) 13850–13851.
[43] T. Duren, F. Millange, G. Ferey, K.S. Walton, R.Q. Snurr, J. Phys. Chem. C 111 (2016) 15350–15356.
[44] D. Yu, M. Wu, Q. Hu, et al., J. Hazard. Mater. 367 (2019) 456–464.
[45] X. Shi, G. Zhu, S. Qiu, K. Huang, R. Xu, Angew. Chem. 43 (2010) 6482–6485.
[46] T.T. Li, Y.M. Liu, T. Wang, et al., Microporous Mesoporous Mater 272 (2018) 101–108.
[47] Y.X. Gao, J. Xia, D.C. Liu, et al., Chem. Eng. J. 378 (2019) 122118.
[48] Y. Zhang, J. Zhou, J. Chen, et al., J. Hazard. Mater. 392 (2020) 122315.
[49] X. Liao, F. Wang, Y. Wang, et al., Appl. Surf. Sci. 509 (2020) 145378.
[50] J.T. Tang, J.L. Wang, Environ. Sci. Technol. 52 (2018) 5367–5377.
[51] A.M. Andani, T. Tabatabaie, S. Farhadi, B. Ramavandi, RSC Adv. 10 (2020) 32845–32855.
[52] F. Yin, C. Wang, K. Lin, S. Tong, J. Taiwan Inst. Chem. Eng. 102 (2019) 163–169.
[53] X. Zhang, Y. Yang, W. Huang, et al., Mater. Res. Bull. 99 (2018) 349–358.
[54] Y. An, Y. Liu, H. Bian, Z. Wang, B. Huang, Sci. Bull. 64 (2019) 1502–1509.
[55] P. Ji, T. Drake, A. Murakarni, et al., J. Am. Chem. Soc. 140 (2018) 10553–10561.
[56] B. Yzla, F. Xjlae, C. Jlz, D. Sqw, F. Bxmae, Sci. Total Environ. 787 (2021) 147554.
[57] H. Misran, S.Z. Othman, N. Mahadi, Z. Aspanut, N. Amin, Acta Phys. Pol. A 135 (2019) 1119–1122.
[58] J. Kong, F. Zhu, W. Huang, et al., J. Chromatogr. A 1603 (2019) 92–101.
[59] J.P. Mehta, T. Tian, Z. Zeng, et al., Adv. Funct. Mater. 28 (2018) 1705581–1705588.
[60] G. Wei, Y. Lu, S. Liu, et al., Chin. Chem. Lett. 32 (2021) 497–500.
[61] R. Sabouni, H. Kazemian, S. Rohani, Chem. Eng. Technol. 35 (2012) 1085–1092.
[62] E. Burgaz, A. Erciyes, M. Andac, O. Andac, Inorg. Chim. Acta 485 (2019) 118–124.

[63] Y. Wan, J. Wan, J.R. Zhao, Y. Wang, Y. Liu, Chemosphere 254 (2020) 126798.
[64] Y. Wan, J. Wan, Y. Ma, Y. Wang, T. Luo, Sci. Total Environ. 701 (2020) 134801–134806.
[65] B.N. Bhadra, D.K. Yoo, S.H. Jhung, Appl. Surf. Sci. 504 (2020) 144348.
[66] S.C. Miao, Z.X. Zha, Y. Li, et al., J. Photochem. Photobiol. A: Chem. 380 (2019) 111862.
[67] F. Liu, J. Cao, Z. Yang, W. Xiong, X. Zhong, J. Colloid Interface Sci. 581 (2020) 195–204.
[68] L. He, Y. Dong, Y. Zheng, et al., J. Hazard. Mater. 361 (2019) 85–94.
[69] Y. Gong, B. Yang, H. Zhang, X. Zhao, J. Mater. Chem. A 6 (2018) 23703–23711.
[70] R. Hejazi, A.R. Mahjoub, A.H.C. Khavar, Z. Khazaee, J. Photochem. Photobiol. A: Chem. 400 (2020) 112644.
[71] X.Y. Guo, C.F. Kang, H.L. Huang, et al., Micro. Meso. Mater. 286 (2019) 84–91.
[72] S.W. Lv, J.M. Liu, N. Zhao, C.Y. Li, S. Wang, Sep. Purif. Technol. 253 (2020) 117413.
[73] Z.C. Li, X.M. Liu, W. Jin, et al., J. Colloid Interface Sci. 554 (2019) 692–704.
[74] J. Lin, H. Hu, N. Ga, et al., J. Water Process Eng. 33 (2020) 101010.
[75] Y. Dong, T. Hu, M. Pudukudy, H. Su, Q. Jia, Mater. Chem. Phys. 251 (2020) 123060.
[76] F.X. Wang, C.C. Wang, X.D. Du, et al., Chem. Eng. J. 429 (2022) 132495.
[77] B.K. Huang, Z.L. Wu, H.Y. Zhou, et al., J. Hazard. Mater. 412 (2021) 125253.
[78] R.S. Kumar, S.S. Kumar, M.A. Kulandainathan, Micro. Meso. Mater. 168 (2013) 57–64.
[79] L.D. Ji, J. Wang, K.B. Wu, N.J. Yang, Adv. Funct. Mater. 28 (2018) 1706961.
[80] P. Arul, N.S.K. Gowthaman, S.A. John, M. Tominag, Electrochim. Acta 354 (2020) 136673.
[81] X. Tao, W. Cong, L. Huang, D. Xu, J. Alloys Compd. 805 (2019) 1060–1070.
[82] K. Uma, G.T. Pan, T.C.K. Yang, Materials 10 (2017) 610.
[83] R.P. Ye, L. Lin, C.C. Chen, et al., ACS Catal. 8 (2018) 3382–3394.
[84] W. Liang, D.M. D'Alessandro, ChemPhysChem 49 (2013) 3706–3708.
[85] G.A. Tompsett, W.C. Conner, K.S. Yngvesson, ChemPhysChem 7 (2010) 296–319.
[86] Z. Ni, R.I. Masel, J. Am. Chem. Soc. 128 (2006) 12394–12395.
[87] Y. Yoo, Z. Lai, H.K. Jeong, Micro. Meso. Mater. 123 (2009) 100–106.
[88] S. Sajjadi, A. Khataee, N. Bagheri, et al., J. Ind. Eng. Chem. 77 (2019) 280–290.
[89] N. Khan, I.J. Kang, H.Y. Seok, et al., Chem. Eng. J. 166 (2011) 1152–1157.
[90] M. Safaei, M.M. Foroughi, N. Ebrahimpoor, et al., TrAC Trends Anal. Chem. 118 (2019) 401–425.
[91] T. Xia, Y. Lin, W.Z. Li, M. Ju, Chin. Chem. Lett. 32 (2021) 2975–2984.
[92] S. Gowniak, B. Szczniak, J. Choma, M. Jaroniec, Mater. Today 46 (2021) 109–124.
[93] H. Ali-Moussa, R.N. Amador, J. Martinez, et al., Mater. Lett. 197 (2017) 171–174.
[94] L. Wu, C.C. Wang, H.Y. Chu, et al., Chemosphere 280 (2021) 130659.
[95] E. Brillas, I. Sirés, M.A. Oturan, Chem. Rev. 109 (2009) 6570.
[96] D. Mantzavinos, E. Psillaki, J. Chem. Technol. Biot. 79 (2004) 431–454.
[97] S.R. Pouran, A.A.A. Raman, W.M.A.W. Daud, J. Cleaner Prod. 64 (2014) 24–35.
[98] A.D. Bokare, W. Choi, J. Hazard. Mater. 275 (2014) 121–135.
[99] M. Cheng, L. Hu, D. Huang, et al., Coordin. Chem. Rev. 368 (2018) 80–92.
[100] E. Andris, R. Navrátil, J. Jašík, et al., J. Am. Chem. Soc. (2017) 2757–2765.
[101] H. Lv, H.Y. Zhao, T. Cao, et al., J. Mol. Catal. A: Chem. 400 (2015) 81–89.
[102] C. Gao, S. Chen, X. Quan, H. Yu, Y. Zhang, J. Catal. 356 (2017) 125–132.
[103] A.N. Pham, G. Xing, C.J. Miller, T.D. Waite, J. Catal. 301 (2013) 54–64.
[104] D.Y. Xu, F. Cheng, Q. Lu, P. Dai, Ind. Eng. Chem. Res. 53 (2014) 2625–2632.
[105] H. Lee, H.J. Lee, D.L. Sedlak, C. Lee, Chemosphere 92 (2013) 652–658.
[106] D.A. Nichela, A.M. Berkovic, M.R. Costante, et al., Chem. Eng. J. 228 (2013) 1148–1157.
[107] Y. Xiong, L.Y. Che, Z.Y. Fu, P.Y. Ma, Adv. Powder Technol. 29 (2018) 1331–1338.
[108] Q. Wu, H.P. Yang, L. Kang, Z. Gao, F. Ren, Appl. Catal. B: Environ. 263 (2020) 118282.
[109] H.T.T. Nguyen, V.P. Dinh, Q.A.N. Phan, V.A. Tran, T.D. Nguyen, Mater. Lett. 279 (2020) 128482.
[110] H.Y. Zhao, Y. Chen, Q.S. Peng, Q.G. Wang, G.H. Zhao, Appl. Catal. B: Environ. 203 (2017) 127–137.
[111] Z. Ye, J.A. Padilla, E. Xuriguera, E. Brillas, I. Sirés, Appl. Catal. B: Environ. 266 (2020) 118604.
[112] X. Zhou, D. Xu, Y. Chen, Y. Hu, Chem. Eng. J. 384 (2020) 123324.
[113] H. Chen, Y. Liu, T. Cai, W. Dong, T. Li, ACS Appl. Mater. Interfaces 11 (2019) 28791–28800.
[114] Y. Jiang, Z. Xiong, J. Huang, et al., Chin. Chem. Lett. 33 (2022) 415–423.
[115] C. Zhang, D. Guo, T. Shen, X. Hou, Q. Hu, Colloid. Surf. A 589 (2020) 124484.
[116] Q. Zhao, J. Wang, Z. Li, Y. Guo, G. Guan, J. Photochem. Photobiol. A: Chem. 399 (2020) 112625.
[117] C. Chen, L. Xu, J.b. Huo, et al., Chem. Eng. J. 391 (2020) 123552.
[118] J. Huang, X. Zhang, H. Song, et al., Appl. Surf. Sci. 441 (2018) 85–98.
[119] D. Yu, L. Li, M. Wu, et al., Appl. Catal. B: Environ. 251 (2019) 66–75.
[120] H. Chen, J.L. Wang, J. Hazard. Mater. 403 (2021) 123697.
[121] Z. Xiong, Y. Jiang, Z. Wu, G. Yao, B. Lai, Chem. Eng. J. 421 (2021) 127863.
[122] Z. Wu, Y. Wang, Z. Xiong, et al., Appl. Catal. B: Environ. 277 (2020) 119136.
[123] X.H. Yi, H.D. Ji, C.C. Wang, et al., Appl. Catal. B: Environ. 293 (2021) 120229.
[124] J.S. Wang, X.H. Yi, X.T. Xu, et al., Chem. Eng. J. 29 (2021) 133213.
[125] X. Liao, F. Wang, Y. Wang, et al., Appl. Surf. Sci. 503 (2020) 144081–144089.
[126] H. Hu, H. Zhang, Y. Chen, Y. Chen, H. Ou, Chem. Eng. J. 368 (2019) 273–284.
[127] M.W. Zhang, K.Y. Andrew Lin, C.F. Huang, S. Tong, Sep. Purif. Technol. 227 (2019) 115632.
[128] C.Q. Zhu, F.Q. Liu, C. Ling, et al., Appl. Catal. B: Environ. 242 (2019) 238–248.
[129] A.J. Sisi, A. Khataee, M. Fathinia, B. Vahid, J. Mol. Liq. 297 (2020) 111838.
[130] Q. Yang, D. Chen, L. Chu, J. Wang, J. Hazard. Mater. 389 (2020) 122148.